Research Article

Boris Bielek, Daniel Szabó, Josip Klem*, and Kristína Kaniková

Application of physical theory of cavity in the construction of double skin facades

https://doi.org/10.1515/cls-2022-0004
Received Aug 06, 2021; accepted Sep 29, 2021

Abstract: The article deals with the issue of double skin transparent facades as a new technological-operational system of transparent exterior walls. Especially of high-rise buildings, which with its operating modes ingeniously uses a renewable source of solar energy to reduce the energy needs of the building. The basic precondition for the correct function of the double skin facade is its functional aerodynamics in any climatic conditions of the outdoor climate. In the critical state of windlessness, the aerodynamic quantification of a double skin facade is the total aerodynamic resistance of the cavity, which consists of the aerodynamic frictional resistances along the length of the air flow line and local aerodynamic resistances of the cavity. The article analyses the functional aerodynamics on two frequented types of double skin facades with a narrow type and corridor type cavity. At the end it confronts functional aerodynamics with the results of their temperature, aerodynamic and energy regime obtained from in-situ experiments.

Keywords: double skin facade, double skin facade cavity, renewable energy source, functional aerodynamics

1 Introduction

At the end of the 20th century, double skinned transparent facades began to be applied in the facade technology of buildings in the developed countries of the world. Construction of double skin facades is based on the theory of physical cavities [1, 2]. As a rule, it is basically an energy impact cavity, the primary function of which is energy. In its integrated functions, the double skin facade system also represents a very important indirect - isolated passive solar system if the flow of medium - air is realized by natural convection, or a hybrid solar system if the flow of medium - air is forced. In both cases, this solar system works on the principle of a simple solar collector [1] – Figure 1. Glass system (single or double) of exterior transparent wall has the function of the solar radiation collector separating the cavity from the exterior. The function of the absorber is the surface and the accumulator is the mass of the inner heat storage wall of the composite structure in its opaque part, separating the cavity from the core of the building and also the shade in front of the transparent surfaces. The function of the regulator and distributor of this solar system is a complex mechanism of air holes, vents, blinds and ducts. It is based on the theory of aerodynamics, providing operational - functional modes of the facade, either with the influence of subjective factor or at a higher level without it, automated environmental management systems energy processes in an intelligent building.

In the system of a double skin facade, an indispensable element is sun protection (adjustable blinds, pull-out blinds, etc.). Movable shading systems allow connection to a suitable automated control system. This presentation of the intelligent cooperation of the building structure and technical equipment of the building, whose aim is to ensure the required conditions for the creation of an artificial living - architectural environment depending on the changing conditions of the outdoor climate, is also inherent in a double skin facade.

In any case, the double skin facade with its energy gains from an alternative energy source - solar radiation, contributes to the energy savings of the building in winter and also by transforming solar radiation into thermal radiation in the cavity of the facade and justified aerodynamics in it, contributes to significant reduction of heat load buildings in summer [1, 3, 4].

The basic precondition for the correct function of the double skin facade is its functional aerodynamics, which ensures the constant movement of the air flow through its cavity in every climatic situation. The critical state is without wind, when the movement of air through the cavity of a double skin facade is based on natural convection.

Boris Bielek, Daniel Szabó, Kristına Kaniková: Slovak University of Technology in Bratislava, Faculty of Civil Engineering, Department of Building Structures
***Corresponding Author: Josip Klem:** Slovak University of Technology in Bratislava, Faculty of Civil Engineering, Department of Building Structures, E-mail: josip.klem@stuba.sk

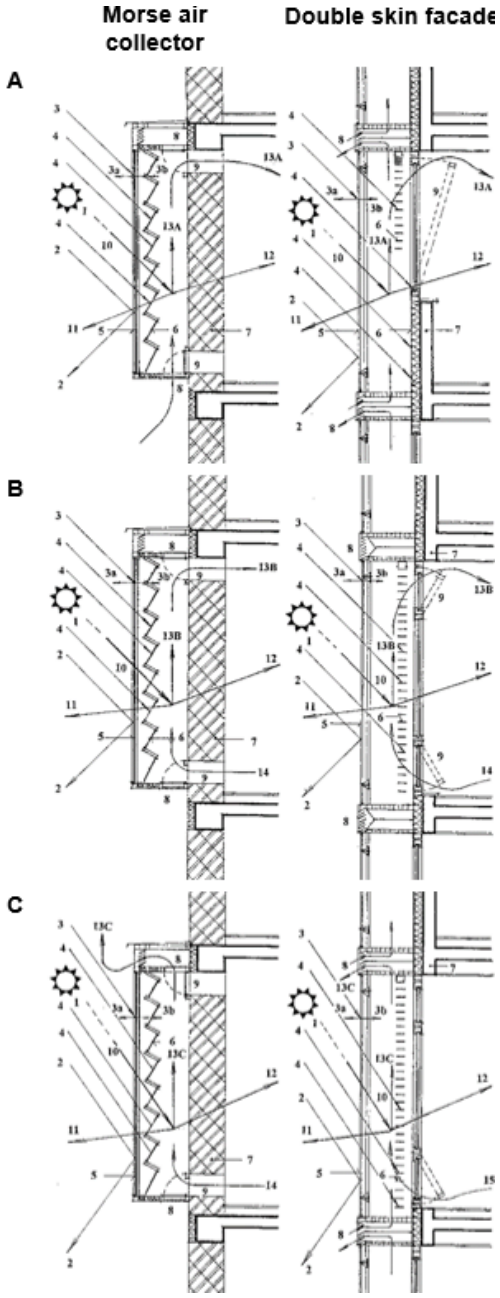

Figure 1: Confrontation of the physical theory of cavity on the principle of a single air collector and a double skin facade A - hot air ventilation mode during the winter period B - circulating air heating mode during the transition period C - passive cooling mode during the summer period 1 - global shortwave solar radiation, 2 - reflected shortwave radiation, 3 - glass absorbed radiation, 3a - longwave radiation radiated to the exterior, 3b - longwave radiation radiated to the interior, 4 - transmitted shortwave radiation transformed in the cavity into longwave thermal radiation 5 - collector, 6 - absorber, 7 - accumulator, 8 - distributor, 9 - regulator, 10 - intensity of transmitted global solar radiation, 11 - heat flow by transmission to the exterior, 12 - heat flow by transmission to the building core, 13A - heat consumed for heating the air in the cavity - used for hot air ventilation, 13B - heat consumed for heating the air in the cavity - used for heating by circulating air, 13C - heat consumed for heating the air in the cavity, which is dissipated to the exterior, 14 - circulating air supply from the building core, 15 - ventilated air supply from the north side - passive cooling.

The functional aerodynamics of the double skin facades (DSF) comes from their correct geometry-construction design (width and effective height of the cavity, geometry of the inlet and outlet openings including the rain louvers and protective screen against birds and insects, type and position of the sun protection device at the cavity and glazing properties), ventilation mode, building orientation, structure and façade design [5]. According to Manz and Frank [6] DSF are in terms of building physics complicated constructions and their construction design must be based on the theory of the natural physical cavities.

Mechanism of the airflow in the double skin transparent cavity can be based on: the natural convection (convective buoyancy) during windless condition, natural convective air flow from the pressure effect form the wind, forced airflow mechanism or combination airflow regime [1, 7]. It is not easy to regulate the natural airflow at the cavity and it is not smooth either, because it depends on external weather condition [7]. Mechanical airflow in the cavity is part of the building heating, ventilation and air condition system (HVAC). It can be used for hot air ventilation preheating a fresh outside air in the cavity [7]. Airflow in the double skin transparent facade cavity is affected with several factors which Hazem et al. [8] divide into the three groups: geometry (inlet and outlet opening dimensions, width of the cavity, angle of the sun protection device and their distance from the inner and outer glazing), material properties (the optical properties of the glazing, the material emissivity, the refraction coefficient and the diffuse fraction) and meteorological parameters (impact of incidence of the solar radiation, angle of incidence of the solar radiation, external temperature, wind direction and velocity).

The dimensions (width of the facade, height of the facade, weight of the cavity, inlet and outlet opening dimensions) and the size of the window opening into the interior have a primary effect on the natural airflow at the cavity [9]. At the larger width of the cavity, the airflow is more turbulent and cause that the velocity at the cavity is increased. There is also smaller increase in the average air temperature in the cavity [10]. The effect of the width of the cavity on the airflow was investigated by Rahmani *et al.* [11] who used simulation programme FloVENT with 5 alternative width (100 mm, 300 mm, 500 mm, 1000 mm and 1500 mm) with typical glazing and reflective glazing at the exterior wall of the DSF. Torres *et al.* [12] used simulation software TAS in which they made a simulation with four different width of the cavity (400 mm, 600 mm, 800 mm a 1000 mm) and with three alternative inlet and outlet opening on the two types of double skin facades (corridor type – one floor and multi-storey facade) to study natural airflow at the cavity. They

have discovered that at the corridor facade type wider cavity (1000 mm) functions better than narrower cavity (400 mm). In the case of multistorey facades on higher floors, there is a considerable increase on the air temperature in the cavity, due to which the convective buoyancy also rises, which also increase the airflow at the cavity.

Gratia and De Herde [13] analysed 4 different width of the cavity (300 mm, 600 mm, 1200 mm and 2400 mm) in Belgium. They used simulation software TAS and concluded that when the cavity width increases, the air temperature in the DSF decrease and the temperature decline in the cavity varies linearly with the size of the inlet and the outlet airflow openings. Radhi *et al.* [14] showed based on simulation, that optimisation of cavity size between 700 mm and 1200 mm can give a balance between solar gain and heat transmission.

Besides the width of the cavity the effective height of the cavity is also determinative due to buoyancy effect during the windless condition. The higher height of the cavity the better buoyancy effect and thus a higher air velocity at the cavity. Ding *et al.* [15] researched the natural cross – ventilation of the building at the south oriented DSF finished by a solar chimney. They made an experiment on a prototype scale model and made a simulation by numerical computational fluid dynamics (CFD). The results showed that the height of the solar chimney should be more than two storeys, in order to increase the airflow rate in the cavity and achieve a positive distribution of pressure differences (between indoor and outdoor).

For the ventilation efficiency of the DSF the inlet and outlet airflow opening are significant. During colder periods of the year the smaller openings are more appropriate to minimalize heat loss by convection, while in warmer periods of the year the larger ones are more suitable to minimize the risk of overheating. The larger area for the inlet and outlet openings reduces the airflow resistance which leads to a larger amount of airflow into the cavity. The size of the inlet opening (actual dimensions including associated components in these openings) has direct effect on the natural airflow and maximizing the area of the outlet opening at the upper part of the DSF assists with the higher airflow velocities [5, 9, 16]. According to Tao *et al.* [9] the optimal height of the opening is about 0.2 – 0.3 m. In addition to the size of the openings, the associated components in these openings also have an effect on the air flow, such as grids at the inlet and outlet of the air distribution ducts, floor and ceiling grilles of the distribution ducts. Increase the area of the vent openings leads to a laminar airflow with higher velocity [10]. Torres *et al.* [12] researched the effects of the dimensions of the inlet and outlet air opening on the facades with corridor type with an effective height identical to one floor and multistorey facade and concluded that with increasing area of the openings in the exterior facade, the intensity of the airflow at the cavity caused by the chimney effect increases. Gratia and De Herde [13] analysed size of the openings on the facade during four sunny days (March, June, September, December) and concluded that the decrease in air temperature in the cavity did not change linearly with increasing size of the inlet and outlet opening.

The airflow in the DSF cavity is significantly affected by the sun protection device situated at the cavity. Mingotti [16] claims that properly designed sun protection device at the DSF exposed to solar radiation in warm sunny seasons helps airflow. In case of intensive solar radiation during warm summer days there may be an excessive increase in air temperature in the cavity, which can also have a negative effect on the lifetime of the components situated in the cavity [16]. Gratia and De Herde [17] found out that when the sun protection device is activated, there may not be sufficient airflow in the cavity. Published works [5, 7, 8] say that the heat absorbed on the surface of the sun protection device from the solar radiation increase the air temperature and chimney effect at the cavity. Barbosa and Ip [5] and Jiru [7] have written about the suitable location of sun protection device in the cavity. According to them the shading device located in the middle of the cavity allows a smoother flow on both sides of the shading device and ensure a lower surface temperature on the inner glazing. When the shading device is placed closer to the inner wall, it may cause a risk of heat transfer to the interior (it could be desirable in winter), at this position the turbulent boundary layer caused by the blinds overlaps with the turbulent boundary layer of the glass surface and the temperature at the cavity rises. Jiru [7] claims that the angle of the slat has a lower effect on the temperature distribution then the position of the blinds and that by changing the angle of the slat the curves of the velocity profiles of the airflow in the cavity are slightly shifted. Barbosa and Ip [5] analysed the appropriate angle position of slat of the shading device. They claim that in terms of air circulation, it is more suitable if the slats are in the vertical position, in horizontal position they cause obstacles to the airflow at the cavity. Hazem [8] wrote about the ideal angle of the slat in terms of the heat flux transmitted to the indoor environment. Safer *et al.* [18] analysed the effect of the position of the air inlet and outlet openings through 2D configuration DSF according to the slat angle inclination and the location of the blinds in the cavity. Gratia and De Herde [19] studied the effect of the location and colour of the shading device in the cavity on the cooling demand of the office building. The results showed that the position of the blinds in the cavity and

their colour influence the surface temperature of the inner glazing. Ji *et al.* [20] researched the effect of the slat angle of the shading device on the airflow at the DSF cavity using CFD simulations in 2D, which they compared with experimental measurement and predictions from the nodal model. The results showed that presence of the blinds at the cavity leads to 35% reduction of the natural airflow in the cavity and 75% reduction of the heat load of the interior. Small changes of the convective heat transfer coefficient were caused by the rotation of the blinds to various angles. Pappas a Zhai [21] wrote that when choosing the type of the shading device, it should be considered how the device will affect airflow in the cavity and it should also be taken into account the colour of the shading device and thus its ability to absorb solar gain that will subsequently radiate from it. Eicker *et al.* [22], compared an effect of a shading device on the indoor thermal comfort in the mild climate in Stuttgart, Germany, on a single skin facade with external shading device and on a DSF with a shading device at the cavity. The results showed that the shading device can effectively reduce the total solar energy transmission to the building in summer period even with slightly opened blinds, for both cases simple and double skin facade. The highest energy priority is to reduce shortwave solar radiation, which is the dominant heat flux. Poirazis [23] says that the choice of the suitable type of the glazing and shading device is decisive for the proper function of DSF. The glazing properties (absorption, reflection, and convection) and its geometry can affect the airflow velocity field at the cavity. For more extensive projects it is useful to find the correct combination of glazing and the position of the shading device at the cavity.

Experimental and numerical models and experiments for naturally ventilated facades with shading devices and mechanically ventilated facades are used for study and the optimisation of the DSF [7]. Significant process has been made in terms of evaluation methods, in particular advances in analytical tools for computational fluid dynamics (CFD), such as analytical and lumped models, non-dimensional analysis, network models, control volume models, zonal models, and computational fluid dynamics (CFD), which allows a better understanding of the complex behaviour of DSF and its interactions with the building without resorting to expensive experiments [5, 24]. The evaluation software tools should meet all three levels of modelling: spectral optical model (using the spectral method), thermodynamic and fluid dynamics (using CFD) and the building energy simulation (using building energy simulation tools). Compared to nodal models, which are often used in building design, this method significantly increases the reliability of prediction [6]. Pappas and Zhai 2008 [21] used in their research the combination of building energy simulation and CFD programmes. Alberto [10] performed simulation used DesignBuilder software with EnergyPlus integration, in which he evaluated the effects of geometry, airflow trajectory, width of the cavity, areas of the facade openings and glazing type on facade performance. Jiru and Haghighat [25], applied a zonal approach for airflow modelling and air temperature at the ventilated DSF. They used equitation of zone airflow and power low for the airflow calculation with integrated shading device. For temperature distribution in the DSF system they used the energy equitation in the zone. The calculated temperature distributions were verified using measured values and parametric studies. Von Grabe [26], developed simulation algorithm for the thermal behaviour and airflow characteristics of DSF with an integrated shading device. In order to determine the degree of accuracy of the algorithm, a double facade has been monitored under controlled conditions and the results have been compared with the predicted values for several design situations.

2 Methods

2.1 Aerodynamic quantification of double skin facade

To work properly, double skin facade has to have functional aerodynamics, which means a constant flow of the air through its cavity in every climatic condition.

The aerodynamic quantification of a double skin transparent facade is its total aerodynamic resistance Z (-), in which:

- aerodynamic frictional resistances along the length L (m) of the airflow line Z_l (-) along the double skin facade height of section H (m) characterized by a coefficient of friction resistance $\bar{\lambda}$ (-),
- local aerodynamic resistances Z_m (-) characterized by aerodynamic coefficients of local resistances ξ (-)

$$Z = 1 + \left(\sum Z_1 + \sum Z_m\right) = 1 + \sum \frac{\bar{\lambda} \cdot (H + b)}{D_h} + \sum_{x=1}^{10} \xi_x \quad (-) \tag{1}$$

where:
$\sum Z_l$ - sum of the frictional resistances along the height of the cavity (-),
$\sum Z_m$- sum of the local aerodynamic resistances (-),
H - effective height of the cavity (m),
b - width of the cavity (m),

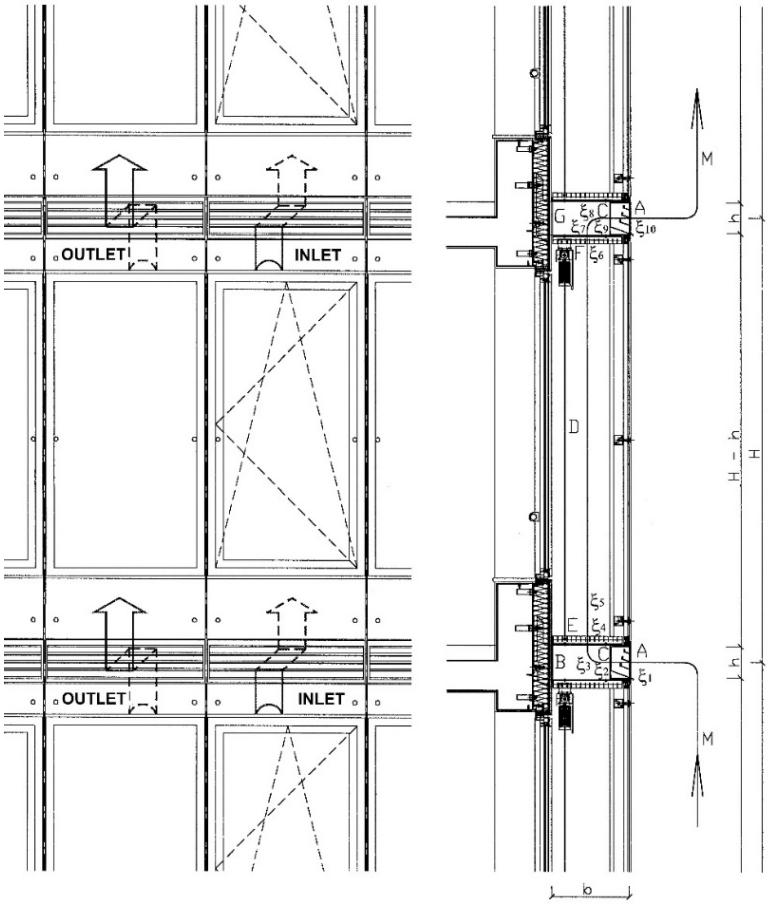

Figure 2: Basic scheme for the definition and quantification of aerodynamic resistances of double skin transparent facade with open circuit A – convection anti rain or aerodynamic shutter, B – inlet air channel, C – bird and insect net, D – cavity of climate facade, E – walkable removable – openable grate, F – floor grate, G – outlet air channel, H – height of the cavity section (m), h – height of the openings of the distribution air channels (m), b – width of the cavity, L – length of the cavity section (m), M – air flow trajectory. ξ_x - aerodynamic coefficient of local resistance of airflow, in particular: ξ_1 - at inlet on aerodynamic louvers "A", ξ_2 - on protective screen "C" at inlet, ξ_3 - where flow direction changes from inlet channel "B" to the cavity "D", ξ_4 - on grille - grid "E" during flow from inlet channel "B" to the cavity "D", ξ_5 - upon sudden increase in diameter during movement of airflow from inlet channel "B" to cavity "D", ξ_6 - on grid "F" during flow from cavity "D" to outlet channel "G", ξ_7 - upon sudden decrease in diameter during movement of airflow from cavity "D" to outlet channel "G", ξ_8 - upon change of direction of movement from cavity "D" to outlet channel "G", ξ_9 - on protective screen "C" at outlet, ξ_{10} - on aerodynamic louvers "A" at outlet.

$\overline{\lambda}$ - coefficient of the friction along the height of the cavity (-), $\bar{\lambda}$ = f(Re), Re (-) is Reynolds number, which gives the ratio of inertial forces and viscous forces acting on the flow of liquids and its value determines whether fluid flow is laminar or turbulent,

ξ_x - aerodynamic coefficients of local resistances along the height of the air flow trajectory through the cavity (-) as explained in Figure 2,

D_h - aerodynamic diameter of the cavity (m).

If the total aerodynamic drag of the cavity is less than the force of the convective buoyancy of the air, then in each climatic condition the air moves in the cavity of the double skin facade.

2.2 Quantification of aerodynamic resistances of double skin facade

The methodology of quantification of aerodynamic resistances of the cavity of a double skin facade will be documented on the facade according to Figure 2. This is a quantification of two basic types of aerodynamic drag:

- aerodynamic frictional resistance along the height of the section of the double skin facade $\sum Z_l = \sum \frac{\bar{\lambda}\cdot(H+b)}{D_h}$ (-),

- local aerodynamic resistances along the height of the moving air stream line of the double skin facade $\sum Z_m = \sum_{x=1}^{10} \xi_x$.

The coefficient of friction resistance along the height of the section of the double skin facade $\bar{\lambda}$ (-) - Figure 3,

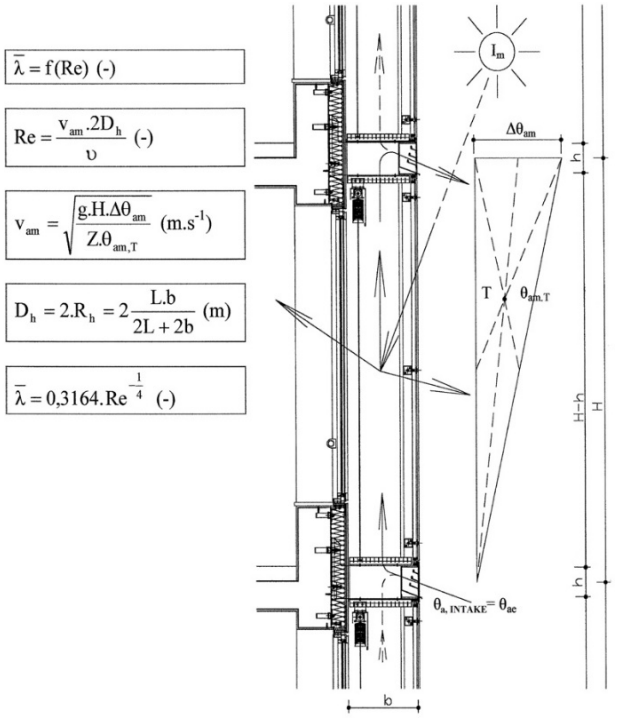

Figure 3: Coefficient of friction resistance along the height of the trajectory of the convective air flow (Re - Reynolds criterial number (-),v_{am} – air flow velocity in the cavity (m/s), ν – coefficient of kinematic viscosity of air (m^2/s), g – gravitational acceleration coefficient (9,81 m/s^2), $\Delta\Theta_{am}$ – temperature increase in the cavity (K), $\Theta_{am,T}$ – temperature in the centre mass point of the triangle surface A = f(H,$\Delta\Theta_{am}$) (°C)).

is determined from the graphical dependence showed on Figure 4. for Reynolds number:

$$Re = \frac{v.2D_h}{\nu} \tag{2}$$

To quantify it, we need to know:

– aerodynamic diameter of the cavity D_h (m). We determine it using the definition of the aerodynamic radius:

$$R_h = \frac{S}{O} = \frac{L.b}{2L+2b}(\mathrm{m}) \tag{3}$$

$$D_h = 2.R_h(\mathrm{m}) \tag{4}$$

– velocity of convective air flow in (m/s). This value is determined from the known temperature differences between the air entering and leaving the cavity $\Delta\Theta_{am}$ (K) and the known temperature at the centre of linear gradient of the cavity $\Theta_{am,\,CENTR}$ (°C), by:

$$\mathrm{Vam} = \sqrt{\frac{g \cdot H \cdot \Delta\theta_{am}}{Z \cdot \theta_{am,CENTR}}} \tag{5}$$

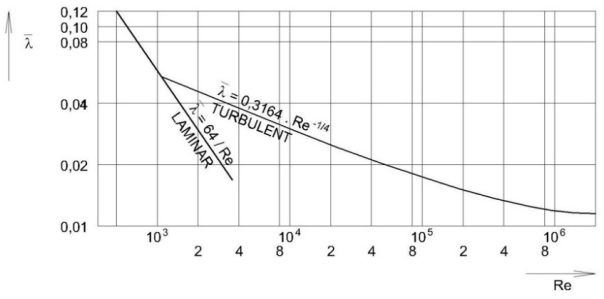

Figure 4: Graphic representation of a coefficient of friction as a function of the cavity height $\bar{\lambda} = f(Re)$.

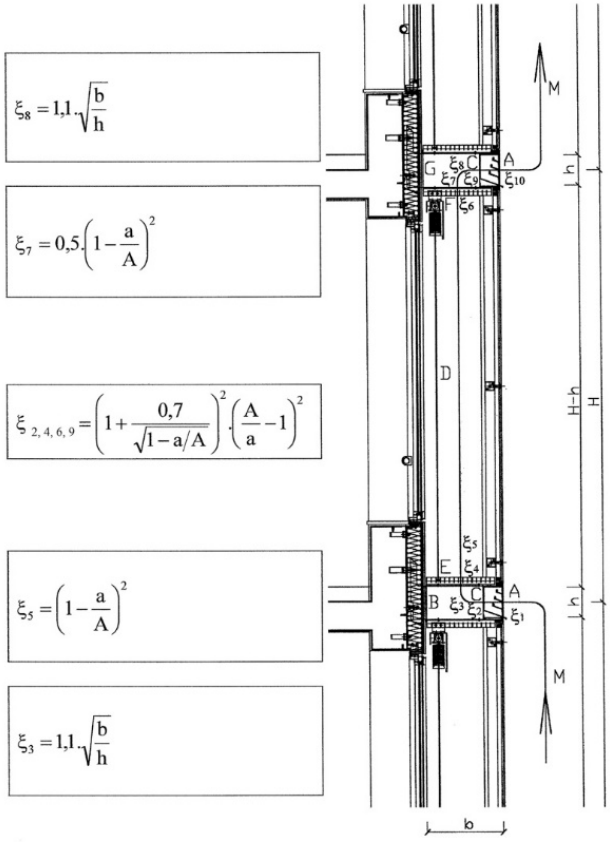

Figure 5: Aerodynamic coefficients of local resistances ξ_2, ξ_3, ξ_4, ξ_5, ξ_6, ξ_7, ξ_8, ξ_9 (-) in the trajectory of air flow (a – net area opening for air movement, A – total area of the air inlets including its solid parts, b – planar width of the rectangular cross-section, h – height of rectangular cross section).

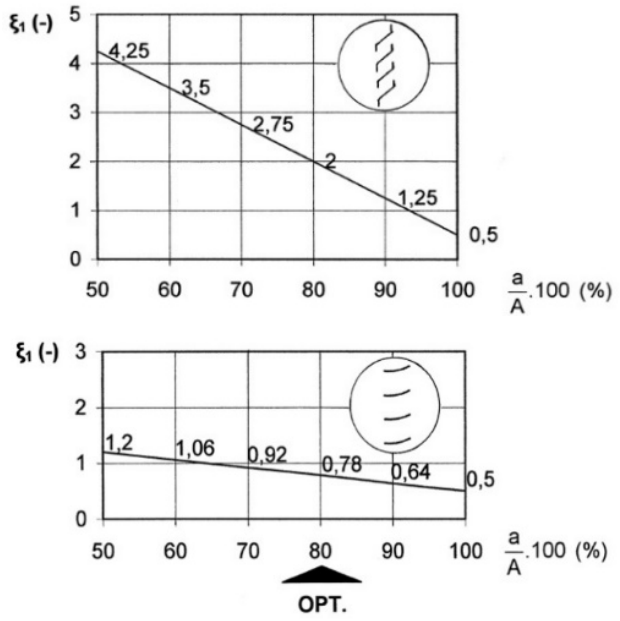

Figure 6: The local aerodynamic drag of the air flow at the inlet part. Upper picture illustrates the conventional rain screen louvers. Lower picture shows aerodynamic louvers (a – net opening area for air flow, A – total area of the inlet air, including the louvers).

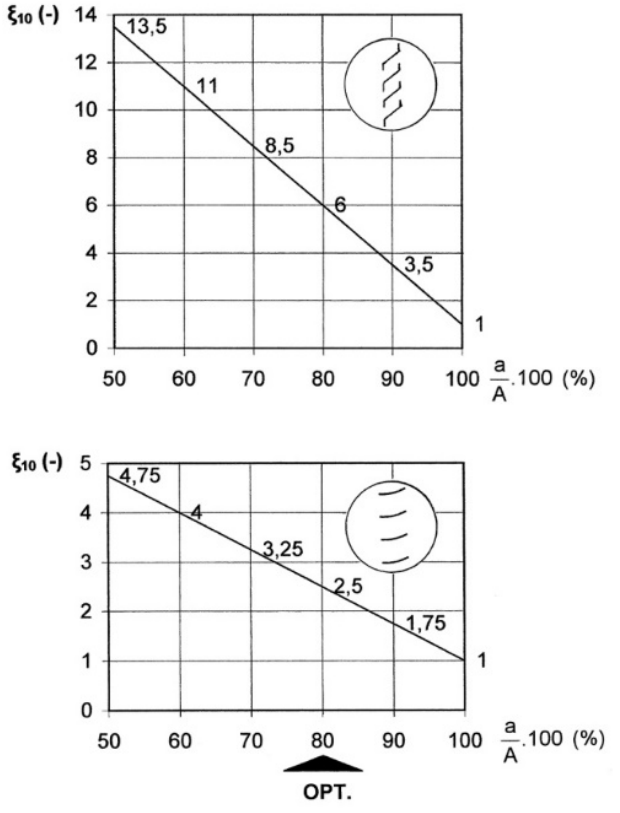

Figure 7: The local aerodynamic drag of the air flow at the outlet part. Upper picture shows conventional rain screen louvers. Lower picture illustrates aerodynamic louvers (a – net opening area for air flow, A – total area of the inlet air, including the louvers).

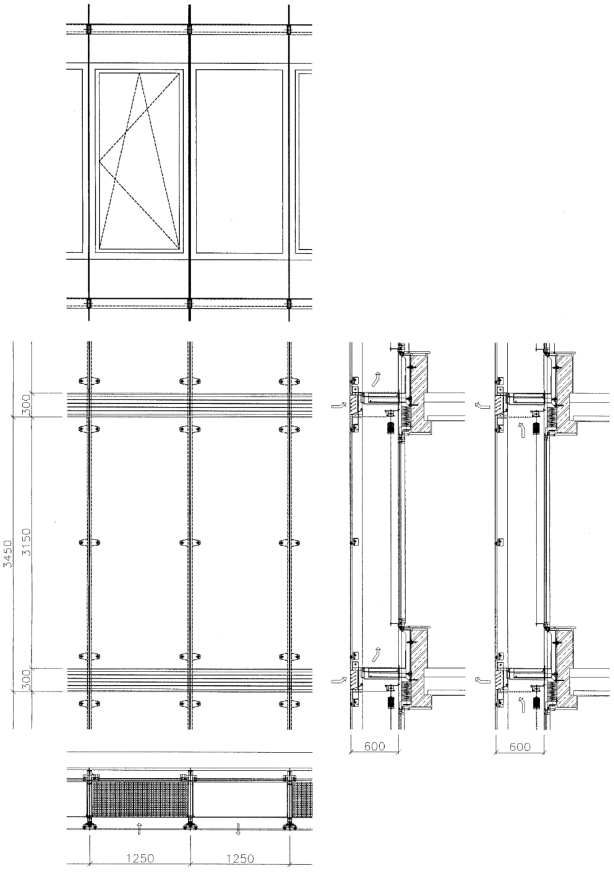

Figure 8: Basic geometry of a double skin facade.

– kinematic viscosity coefficient of air ν (m^2/s).

Coefficients of local resistances along the height of the moving line of the air flow of the double skim facade – Figure 5, is determined as:

– aerodynamic coefficient of local resistance ξ_1 (-) of air flow at the entrance with louver "A" – Figure 2. which characterizes the swirling of the air flow at the entrance to the supply channel "B" is determined from the graphical dependences in Figure 6 depending on the type of blinds.
– aerodynamic coefficients of local resistance ξ_2, ξ_4, ξ_6, ξ_9 (-) of air flow on the mesh or grate – Figure 2, which characterize the swirling of the air flow when overcoming the mesh or grate, we determine as:

$$\xi_{2,4,6,9} = \left(1 + \frac{0,7}{\sqrt{1 - a/A}}\right)^2 \cdot \left(\frac{A}{a} - 1\right)^2 \quad (6)$$

where:
A – the total area of the net or grate, including their fixed surfaces (m^2)
a – area of the air openings (m^2).

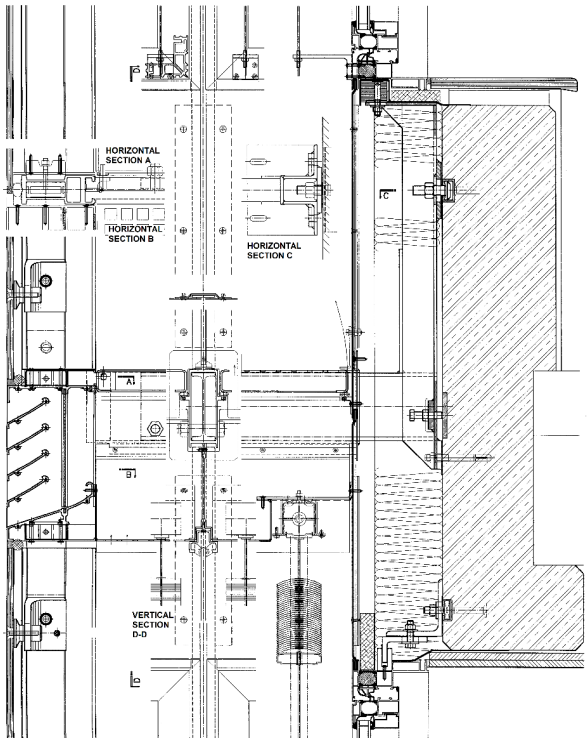

Figure 9: The characteristic vertical section of the double skin facade showing the compatibility of its basic and complementary theoretically justified structural elements and details into a complete structural system.

– aerodynamic coefficients of local resistance ξ_3, ξ_8 (-) of air flow when changing direction – Figure 2, which characterizes the vortex - impact of air flow when changing direction, we determine as:

$$\xi_{3,8} = 1,1.\sqrt{\frac{b}{h}} \tag{7}$$

where:
b – plan width of the rectangular cross-section (m)
h – height of the rectangular cross-section (m) (for $\frac{b}{h} \leq 1$)

– aerodynamic coefficient of local resistance ξ_5 (-) at sudden widening of the cross-section during the movement of the air flow from the supply duct "B" to the cavity "D" – Figure 2, which characterizes the swirling of the air stream at sudden widening of the cross-section between the supply duct "B" and the cavity "D" is determined by the relation:

$$\xi_5 = \left(1 - \frac{a}{A}\right)^2 \tag{8}$$

where:
A – larger extended cross - sectional area (m^2),
a – smaller original cross - sectional area (m^2).

– aerodynamic coefficient of local resistance ξ_7 (-) in case of sudden narrowing of the cross-section during the movement of the air stream from the cavity "D" to the exhaust duct "G" – Figure 2, which characterizes the swirling of the air stream in case of sudden narrowing of the cross-section “G" is determined by the relation :

$$\xi_7 = \left(1 - \frac{a}{A}\right)^2 \tag{9}$$

where the meaning of the symbols is the same as in relation (8).

– aerodynamic coefficient of local resistance ξ_{10} (-) of air flow at the outlet with louver "A" – Figure 2, which characterizes the turbulence of the air flow at the outlet of the drainage channel "G" is determined from the graphical dependence on Figure 7 again depending on the type of blinds.

2.3 Alternative possibilities of construction for double skin facades

From the point of view of its fundamental concept, a double skin facade can be developed in broad modifications of its construction, which influences: choice of cavity geometry (width and height zoning), approach to cavity aerodynamics (natural or forced air movement), choice of glass system of suspended transparent wall (single or double, without or with other special functions) and a conceptual approach to the use of the physical functions of the cavity (open or closed circuit facades). The wide variability of these factors determines the wide variability of facades of this kind.

The current trend in the design of project applications of double skin facades, corresponding to the current level of theoretical knowledge of the problem, focuses on double skin facades with the corridor type cavity (width 500 mm - 1500 mm) with section height identical to the height of one floor and also economical double skin facades with the slot type cavity (width 100 mm - 300 mm) with the height of the section also identical with the height of one floor, realized in the form of a spatial completed part - element.

Let’s demonstrate the structural creation of the two development types of double skin facades, including their physical assessment based on in-situ experiments.

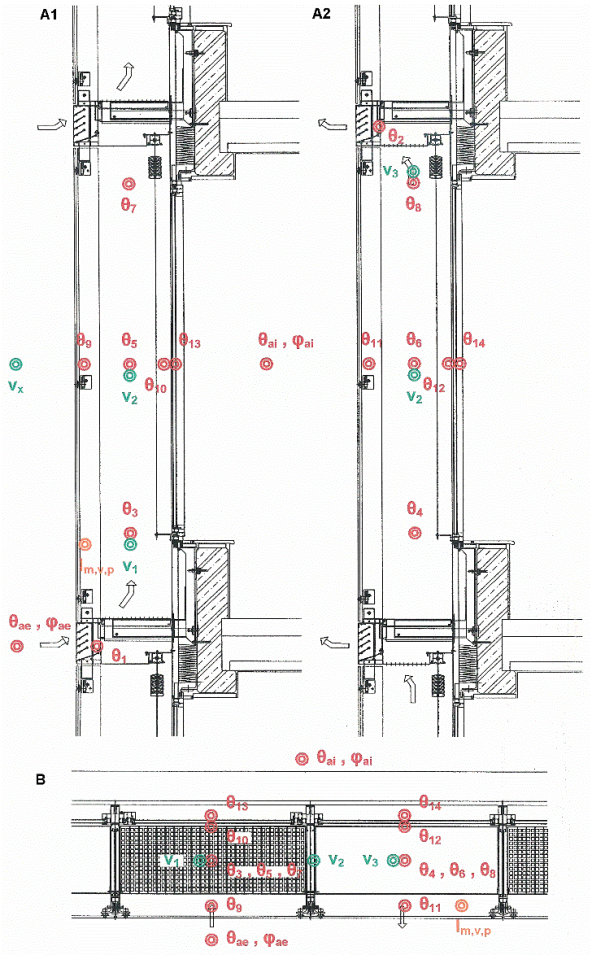

Figure 10: Examined physical parameters of the double skin transparent facade. A1 – vertical section – inlet module, A2 – vertical section – outlet module, B – horizontal section through inlet and outlet modules. Θ_x – measuring points for temperature monitoring (°C), v_x - measuring points for monitoring air velocity (m/s), ϕ_a - measuring points for monitoring relative humidity (%) .

2.4 Double skin facade with corridor type cavity

The first example documents the structural creation of a double skin facade with corridor type cavity, width b = 600 mm, with an effective height of the cavity identical to the height of one floor (H = 3450 mm) - Figure 8. The detailed construction solution of the double skin facade is documented in Figure 9. The facade was realized by multi-phase assembly technology.

The airflow in the cavity of the facade is based on natural flow - a combination of natural convection and the effect of wind. The total aerodynamic resistance of the facade was quantified as:

Figure 11: View into the cavity of a double skin facade with installed sensors of physical quantities .

$$Z = 1 + \sum \frac{\bar{\lambda} \cdot (H + b)}{D_h} + \sum_{x=1}^{10} \xi_x = 1 + 0,20 + 14,94 = \\ = 16,14 < 18 = Z_{\text{conv}} \tag{10}$$

which expresses the convective buoyancy of the air in the cavity of a double skin facade. Based on the above, it can be stated that in terms of functional aerodynamics of the cavity, the above-mentioned facade is designed correctly and that airflow through its cavity is ensured in any climatic situation.

We monitored the temperature, aerodynamic and energy regime of the double skin facade for 18 months with an in-situ experiment. The experiment was carried out on 17th floor, 56.3m above the terrain. Orientation of the experimentally examined part of the cavity was SW (240°). The recorded physical parameters of the double skin facade are shown in Figure 10. The view of the installed sensors for measuring physical quantities in the cavity of the facade is documented in Figure 11. From the whole range of results of the in-situ experiment, in this article we will focus on the critical state of windlessness in terms of functional aerodynamics, when the movement of air in the cavity of a double skin facade is based on natural convection. An example of the recording of measured physical quantities

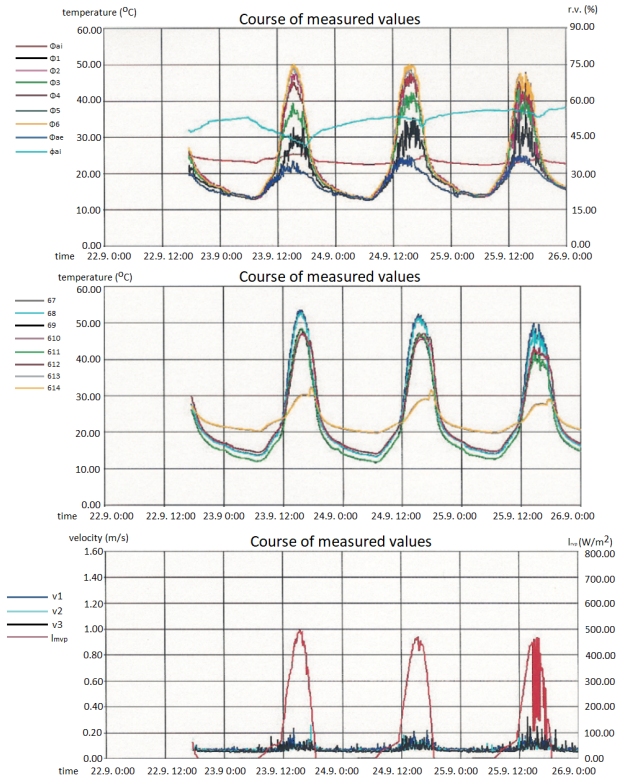

Figure 12: The example of measured values from the experiment for the typical period of clear windless warm weather ($v_W \leq 0.5$ m/s).

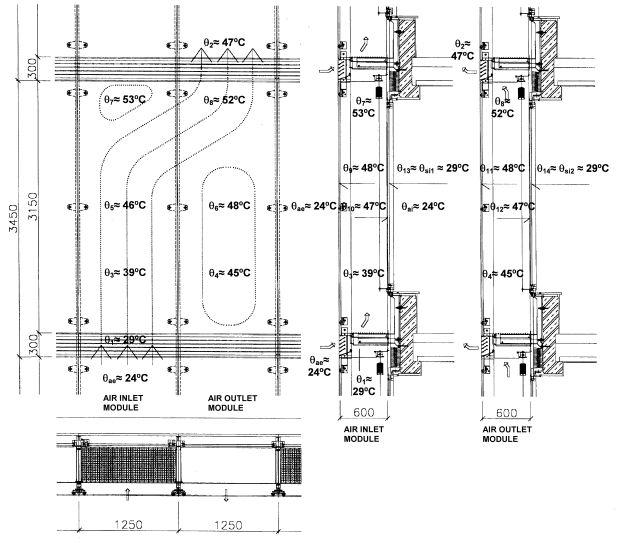

Figure 13: Natural physical cavity of double skin facade. Climate situation: period of clear windless warm weather $v_W \leq 0.5$ m/s. Distribution of characteristic temperatures. Characteristic movement of convective air flow.

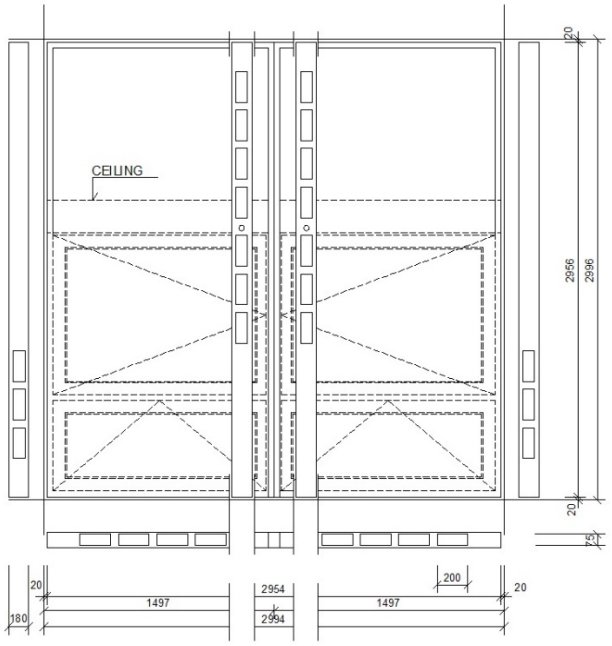

Figure 14: Construction diagram of the double skin facade element with a narrow type cavity.

in the cavity of a double skin facade in the period of clear windless warm weather is documented in Figure 12.

Following the processing – research into the long-term experiments of loads on natural physical cavity of the double skin transparent facade only by effects of outdoor temperatures, relative humidity and effects of global solar radiation (windless) we can state :

- convective airflow occurs in the cavity in every stress interval and its velocity ranges from $0.05 \leq v$ (m/s) $\leq$ 0.2 to 0.3,
- under the effect of global solar radiation (900 - 1800) the convective velocity increases,
- as a result of alternating position of air inlet and air outlet modules the energy regime in the cavity is characterized by inhomogeneity – Figure 13,
- there are 3 characteristic areas for the thermal and aerodynamic regime in the cavity:

• area of increasing temperatures along height of the cavity in the air inlet module – convective air flow movement,

• small area of particularly high temperatures in the upper part of air inlet module of the cavity – stagnation of warm air,

• large area of high temperatures in air outlet module of the cavity – stagnation of warm air – Figure 13.

Based on the results of a long-term in-situ experiment of the physical regime of the mentioned double skin facade,

we can state that in its cavity there is a constant airflow in any climatic situation (even in windless condition). This fact is a confirmation of the correct physical function of the cavity and testifies to the quality design of the facade in terms of its aerodynamic dimensioning.

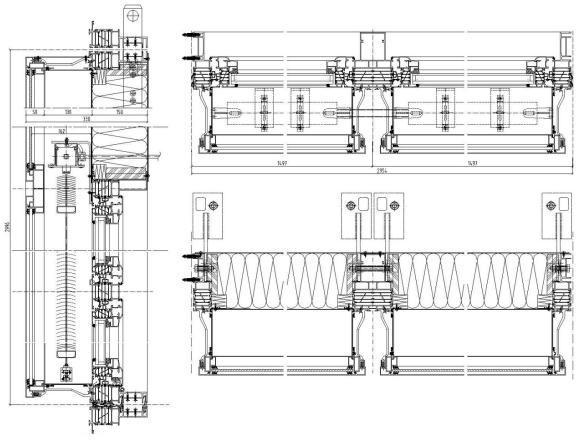

Figure 15: Characteristic sections of the double skin facade element.

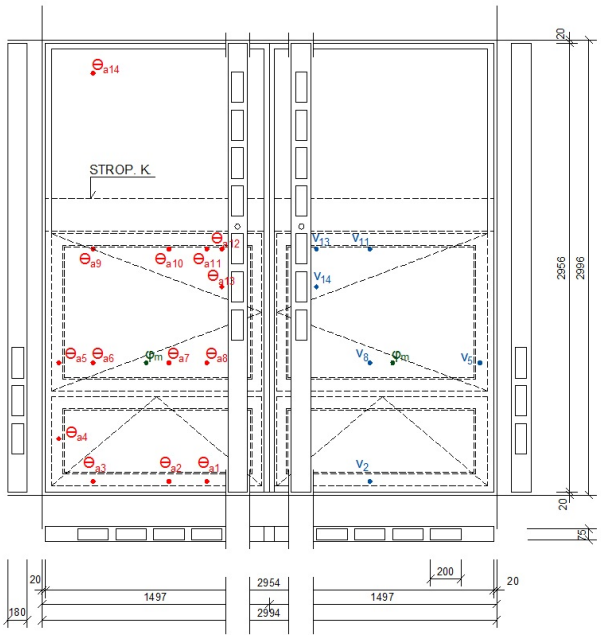

Figure 16: Scheme of distribution of measuring points for measured parameters of the cavity in the completed part of double skin facade Θ_a, x - measuring points for temperature measurement (°C), v_x - measuring points for measuring air velocity (m/s), ϕ_m - measuring points for measuring relative humidity (%).

2.5 Double skin facade with narrow type cavity

The second example documents - the structural creation of a double skin facade of a narrow type cavity, width b = 162 mm, with an effective height of the cavity identical to the height of one floor (H = 3000 mm) – Figure 14. The facade was constructed by a single-phase assembly technology from a spatially assembled part - element. Figure 15 documents a detailed structural solution of the facade element.

The functional aerodynamics of above mentioned double skin facade - the movement of air in the cavity - was based on natural flow - a combination of natural convection and the effect of the wind. Natural physical cavity of the assembled panel of the double skin facade is due to :

- the relative complexity of air inlet and outlet openings – Figure 14,
- relatively small cross-sectional area of these openings ($\sum A_{OPENING} \approx 0{,}05\ m^2$/ per meter of panel,
- geometric disproportion of air on exhaust from the cavity (from two panels and 14 openings of area $\sum A_{OPENING} \approx 0{,}1\ m^2$ – Tab.1, into the collecting channel of cross-sectional area $A_{VERT.CANAL} \approx 0{,}0064\ m^2$) characterized by high coefficients of local aerodynamic resistance of air outlet, and thus a high value of the total aerodynamic resistance of the physical cavity.

Total aerodynamic resistance of the facade was calculated in the value of:

$$Z = 1 + \sum \frac{\bar{\lambda} \cdot (H + b)}{D_h} + \sum_{x=1}^{12} \xi_x = 1 + 0,37 + 12,88 = \\ = 14,25 > 12 = Z_{\text{conv}} \tag{11}$$

which expresses the convective buoyancy of the air in the cavity of a double skin facade. This aerodynamic quantification of the cavity of the double facade is without considering the local resistances on the lowered lamellas of the screening device.

If the quantification of the total aerodynamic resistance of the facade also takes into account the triggered sun protection situated in this cavity, which occupies approximately 1/3 of the cavity and its local aerodynamic resistance represents up to 25% of the total aerodynamic resistance of the cavity of the facade. :

Figure 17: View of the installed sensors for measuring the physical parameters of the cavity of the double skin facade element.

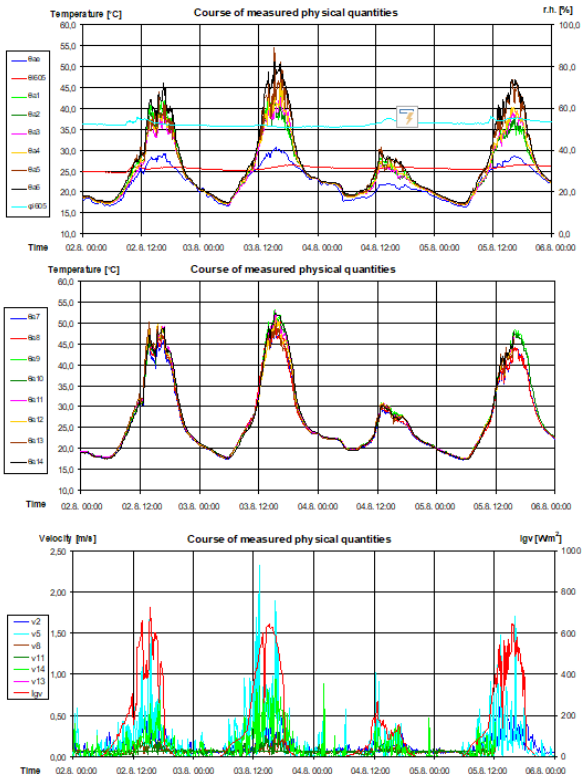

Figure 18: The example of measured values from the experiment for the typical period of nice warm weather.

$$Z = 1 + \sum \frac{\bar{\lambda} \cdot (H + b)}{D_h} + \sum_{x=1}^{14} \xi_x = 1 + 0,37 + 19,11 = \\ = 20,48 \gg 12 = Z_{\text{conv}} \tag{12}$$

Based on the above, it can be stated that from the point of view of functional aerodynamics, the facade mentioned above has a significant problem resulting in the stagnation of air in its cavity during windlessness.

This facade was also subjected to in-situ experiments to verify its physical regime. The experiment was carried out on 6th floor, 22.19 m above the terrain. Orientation of the experimentally examined part of the cavity was SW (240°). The recorded physical parameters of the double transparent facade are shown in Figure 16. The view of the installed sensors for measuring physical quantities in the cavity of the facade is documented in Figure 17. An example of the recording of measured physical quantities in the cavity of a double facade in the period of warm weather is documented in Figure 18.

Based on the results of monitoring the physical regime of the double skin facade from the in-situ experiment, we can state that in the cavity of the facade in certain time periods there is air stagnation, which confirms the theoretical assumption of significantly higher total aerodynamic resistance of the double skin facade than the convective lift force. air in its cavity. This is also supported by the fact that in the scheme of air movement in the cavity according to Figure 19 the measured values of air velocity v_x (m/s) at inlet openings v_2, v_5 (m/s) are significantly higher than at outlet openings v_{13}, v_{14} (m/s) or in the middle of cavity v_8, v_{11} (m/s). As a result, despite the relatively small effective height, there is a significant increase in the air temperature in the cavity in windless conditions – Figure 18 and Figure 20.

As a result of geometric disproportion in cross sections of airflow trajectory through the natural physical cavity of the double skin facade, there is :

- high value of its total aerodynamic resistance, causing stagnation of air in the cavity under still air (aerodynamic resistance of the cavity is higher than convective air buoyancy) [2]
- low airflow rate through the cavity ($q_m \approx 0,04$ kg/s.m « 0,2 kg/s.m = $q_{m,\text{REQUIRED}}$) [1, 3], causing low energy efficiency of the double skin facade.

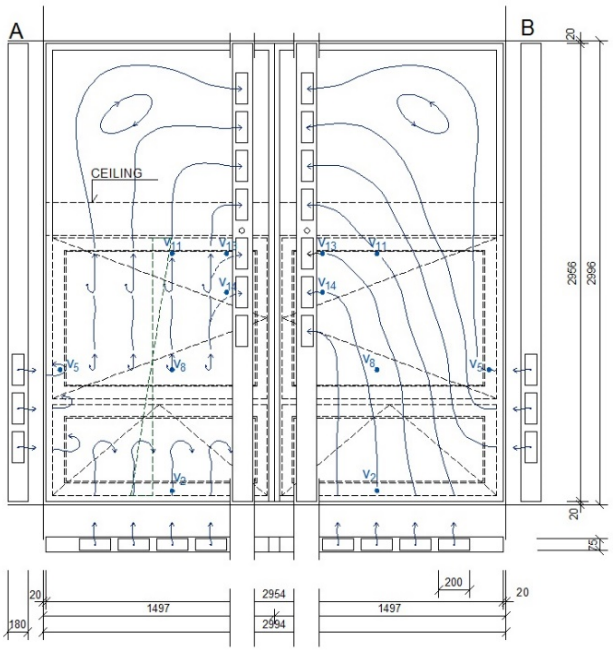

Figure 19: Scheme of air movement in the cavity of a double facade A - windows of the inner wall of the double facade open B - windows of the inner wall of the double facade closed.

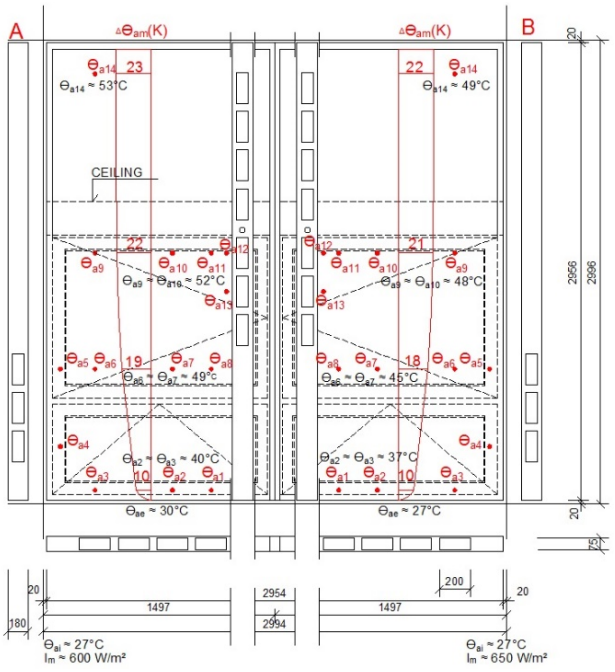

Figure 20: Schemes of air temperature rise in the cavity of a double facade $\Delta\Theta_{am}$ (K). A - windows of the inner wall of the double facade closed B - windows of the inner wall of the double facade open.

These two facts are responsible for high temperature rise in the physical cavity (Figure 15) as well as high air temperatures of indoor climate during the typical summer period. They are caused by underestimation of the physical dimensioning of the double skin facade in two main interrelated and mutually influencing fields, in the field of aerodynamics [1] and in the field of solar thermal technology in buildings [3].

3 Conclusions

Physical-structural dimensioning and design of individual elements and the whole system of a double skin facade is a demanding process, based on the theory of natural physical cavities. The theory of cavities results in a double skin facade in the quantification of the physical regime of its cavity. It is a matter of knowing the aerodynamic, temperature and energy regime in time, while it should be noted that there are strong bonds between them expressed by the laws of physics.

Properly functioning double skin transparent facade has to be able to eliminate the thermal load from shortwave solar radiation through its transformation into long-wave thermal radiation in the physical cavity. Underestimation of functional aerodynamics in the construction and technical design of a double skin facade results in stagnation of air in its cavity, resulting that during the solar radiation there is significant increase in air temperature in the cavity with a negative impact on the temperature inside the building.

Double skin facade with a narrow type cavity are significantly more demanding on their physical-structural dimensioning in terms of their functional aerodynamics than facades with a corridor cavity. This fact is significantly influenced by the sun protection in the form of shading mobile blinds situated in this cavity, which in the lowered state occupies a large part of the cavity and represents a significant increase in the overall aerodynamic resistance of the cavity of the double skin facade. Its local aerodynamic resistance can represent up to 25% of the value of the total aerodynamic resistance of the cavity of the double skin facade.

Acknowledgement: This work was supported by the Scientific Grant Agency of the Ministry of Education, Science, Research and Sport of the Slovak Republic and the Slovak Academy of Sciences in the project VEGA 1/0113/19 and by the Slovak Research and Development Agency under the contract No. APVV-16-0126.

Funding information: The authors state no funding involved.

Author contributions: All authors have accepted responsibility for the entire content of this manuscript and approved its submission.

Conflict of interest: The authors state no conflict of interest.

References

[1] Bielek B, Bielek M, Palko M. Double-skin transparent facades of buildings. 1st volume : History, development, classification and theory of design. Bratislava: Coreal. 2002.
[2] Bielek B, Bielek M, Kusý M, Paňák P. Double-skin transparent facades of buildings. 2nd volume : development, simulation, experiment and design of the facade of the Slovak National Bank building in Bratislava. Bratislava: Coreal. 2002.
[3] Compagno A. Inteligent Glass Facades – Material Practice Design. 1st ed. Basel, Boston, Berlin: Birkhäuser Verlag. 1995.
[4] Oesterle E, Lieb RD, Lutz M, Heusler W. Doppelschalige Fassaden, Ganzheitliche Plannung. München: Callwey Verlag. 1999.
[5] Barbosa S, Ip K. Perspectives of double skin façades for naturally ventilated buildings: A review. Renew Sust Energy Rev. 2014;40:1019-1029.
[6] Manz H, Frank T. Thermal simulation of buildings with double-skin façades. Energy Build. 2005;37(11):1114-1121.
[7] Jiru TE, Taob YX, Haghighat F. Airflow and heat transfer in double skin facades. Energy Build. 2011;43(10):2760-2766.
[8] Hazem A, Ameghchouche M, Bougriou C. A numerical analysis of the air ventilation management and assessment of the behavior of double skin facades. Energy Build. 2015;102:225-236.
[9] Tao Y, Zhang H, Zhang L, Zhang G, Tu J, Shi L. Ventilation performance of a naturally ventilated double-skin façade in buildings. Renew Energy. 2021;167(C):184-198.
[10] Alberto A, Ramos NM, Almeida RM. Parametric study of double-skin facades performance in mild climate countries in J. J Build Eng. 2017;12:87–98.
[11] Rahmani B, Kandar MZ, Rahmani P. How double skin Façade's air-gap sizes effect on lowering solar heat gain in tropical climate? World Appl Sci J. 2012;774–8.
[12] Torres M, Alavedra P, Guzmán A, Cuerva E, Planas C, Raquel C et al. Double skin façades – cavity and exterior openings dimensions for saving energy on mediterranean climate. Build Simul. 2007;198-205.
[13] Gratia E, De Herde A. Greenhouse effect in double-skin facade. Energy Build. 2007;39(2):199-2011.
[14] Radhi H, Sharples S, Fikiry F. Will multi-facade systems reduce cooling energy in fully glazed buildings? A scoping study of UAE buildings. Energy Build. 2013;56:179-188.
[15] Ding W, Hasemi Y, Yamada T. Natural ventilation performance of a double-skin façade with a solar chimney. Energy Build. 2005;37(4):411-418.
[16] ingotti N, Chenvidyakarn T, Woods AW. The fluid mechanics of the natural ventilation of a narrow-cavity double-skin facade. Build Environ. 2011;46(4):807–23.
[17] Gratia E, DeHerde A. Optimal operation of a south double-skin facade. Energy Build. 2004;36(1):41-60.
[18] Safer N, Woloszyn M, Roux JJ. Three-dimensional simulation with a CFD tool of the airflow phenomena in single floor double-skin facade equipped with a venetian blind. Sol Energy. 2005;79(2):193-203.
[19] Gratia E, De Herde A. The most efficient position of shading devices in a double-skin facade. Energy Build. 2007;39(3):364-373.
[20] i Y, Cook MJ, Hanby VI. D. Infield DGG, Loveday DLL, Mei L. CFD modelling of double-skin facades with venetian blinds. J Build Perform Simul. 2007;1(3):185-196.
[21] Pappas A, Zhai Z. Numerical investigation on thermal performance and correlations of double skin façade with buoyancy-driven airflow. Energy Build. 2008;40(4);466-475.
[22] Eicker U, Fux V, Bauer U, Mei L, Infield D. Facades and summer performance of buildings. Energy Build.2008;400(4):600-611.
[23] Poirazis H. Double-skin façades for office buildings–literature review, Report EBD-R-04/3, Division of Energy and Building Design, Department of Construction and Architecture, Lund Institute of Technology. Lund; 2004.
[24] De Gracia A, Castell A, Navarro L, Oró E, Cabeza LF. Numerical modelling of ventilated facades: A review. Renew Sust Energy Rev. 2013;22:539-549.
[25] Jiru TE, Haghighat F. Modeling ventilated double skin façade-A zonal approach. Energy Build. 2008;40(8):1567–1576.
[26] Von Grabe J. A prediction tool for the temperature field of double facades. Energy Build. 2002;34(9):891-899.